International Journal of Computer Vision 42(3), 177–189, 2001

Scale Dependency of Image Derivatives for Feature Measurement in Curvilinear Structures

G.J. STREEKSTRA
Department of Medical Physics, Academic Medical Center, P.O. Box 22700, 1100 DE Amsterdam, The Netherlands
geert@wins.uva.nl

R. VAN DEN BOOMGAARD AND A.W.M. SMEULDERS
Intelligent Sensory Information Systems, Faculty of Science, University of Amsterdam, Kruislaan 403, 1098 SJ Amsterdam, The Netherlands
rein@wins.ura.nl
smeulders@science.ura.nl

Received July 26, 2000; Revised January 31, 2001; Accepted February 6, 2001

Abstract. Extraction of image features is a crucial step in many image analysis tasks. In feature extraction methods Gaussian derivative kernels are frequently utilized. Blurring of the image due to convolution with these kernels gives rise to feature measures different from the intended value in the original image. We propose to solve this problem by explicitly modeling the scale dependency of derivatives combined with measurement of derivatives at multiple scales. This approach is illustrated in methods for feature measurement in curvilinear structures. Results in 3D Confocal Images confirm that modelling of scale behavior of derivatives results in improved methods for center line localization in curved line structures and enables curvature and diameter measurement.

Keywords: feature measurement, scale, image derivatives, curvilinear structures, curvature, center line detection, localization, bias removal, diameter measurement

1. Introduction

The notion of scale at which an image is observed, processed or analyzed has found a profound theoretical basis in linear scale space theory (Koenderink and van Doorn, 1994; Lindeberg, 1994; Sporring et al., 1997). Within this framework it is possible to apply differential geometrical techniques in images that are effectively blurred at a chosen scale σ. To obtain derivatives in the blurred image the original image is convolved with Gaussian derivative kernels. Regularization of the image derivatives by convolution with a Gaussian reduces the noise sensitiveness in the calculation of derivatives and ensures meaningful derivative values even when steep edges in the image are present. Combinations of image derivatives turn out to be powerful tools to extract object features like corners, edges or blobs in a blurred versions of the image (Florack et al., 1992).

Whereas linear scale space theory has reached a high level of mathematical sophistication its translation to quantitative image analysis still needs further development. In current practice the scale of observation is usually either chosen empirically or based on a procedure for automatic scale selection (Lindeberg, 1994; Staal et al., 1999). The final feature extraction is based on measurement of image derivatives at only one scale. However, Gaussian derivative values and therefore also feature estimates depend on the particular

scale selected in the measurement procedure (Deriche and Giraudon, 1993; Kuijper and Florack, 1999; Lindeberg, 1992; van Vliet, 1993). An illustration of this phenomenon is the existence of trajectories which represent the location of critical points as a function of scale (Kuijper and Florack, 1999).

Due to the scale dependency of image derivatives its measurement at a single scale does not solve the inherent conflict between noise suppression and accurate measurement of local derivatives and features of the object in the original image. We propose to solve this dilemma by explicitly modeling the scale dependency of image derivatives resulting from characteristics of objects in the image. We incorporate the notion that without the presence of noise the derivatives calculated at zero scale would be unbiased. Since it is impossible to calculate Gaussian image derivatives at zero scale in a discrete image we utilize measurement of image derivatives at multiple non-zero scales to obtain the desired quantitative information about the object in the original image at zero scale.

In this paper we illustrate the usefulness of scale dependency of image derivatives for feature extraction in images containing curvilinear structures. Features of interest here are center line position, curvature and diameter (Capowsky, 1989; Houtsmuller et al., 1993; Noordmans, 1997; Cesar and Da Costa, 1997; Steger, 1998; Jonk, 1997). The scale dependency of center line location in curved line structures is modeled to investigate the shift in line center position due to curvature. A method to compensate for this shift is developed to improve the estimate of the center line position. The same center line shift is used to estimate the local curvature of the center line. A diameter measurement procedure is presented which is based on the scale dependency of the 0th and the second Gaussian derivatives in the image.

The validity of the line tracing, the curvature measurement and the diameter estimation method is demonstrated by applying the methods to both synthetic images and 3D images of biological structures obtained with a confocal microscope (Brakenhoff, 1997).

2. Tracing Curvilinear Structures

In the modeling of a curvilinear structure a useful criterion for a center line point is to consider it to be part of a structure which length is much larger than its diameter (Lorenz et al., 1997; Koller et al., 1995). Within the framework of differential geometry in Gaussian blurred images this criterion can be effectively utilized for detection of curvilinear structures (Steger, 1998; Lorenz et al., 1997; Koller et al., 1995; Koenderink and van Doorn, 1994; Eberly, 1996; Maintz et al., 1996; Haralick, 1983; Frangi et al., 1999; Sato et al., 1998). The starting point of our tracing procedure is the center line detection method introduced by Steger (Steger, 1998).

2.1. Tracing Procedure

Consider a discrete point $\mathbf{P_d}$ at position in the image close to a center line position. At this position we calculate the Gaussian derivatives up to order 2. For the 3D case the Gaussian derivatives are obtained by convolution of the original image $I(x, y, z)$ with the appropriate Gaussian derivative kernels i.e.

$$\begin{aligned} I(x, y, z, \sigma) &= G(x, y, z, \sigma) * I(x, y, z), \\ I_p(x, y, z, \sigma) &= G_p(x, y, z, \sigma) * I(x, y, z), \\ I_{pq}(x, y, z, \sigma) &= G_{pq}(x, y, z, \sigma) * I(x, y, z). \end{aligned} \quad (1)$$

with

$$\begin{aligned} G(x, y, z, \sigma) &= \frac{1}{(\sqrt{2\pi\sigma^2})^3} e^{-\frac{x^2+y^2+z^2}{2\sigma^2}}, \\ G_p(x, y, z, \sigma) &= \frac{\partial G(x, y, z, \sigma)}{\partial p}, \quad (p = x, y, z), \\ G_{pq}(x, y, z, \sigma) &= \frac{\partial^2 G(x, y, z, \sigma)}{\partial p \partial q}, \\ &\qquad (pq = xx, xy, xz, yy, yz, zz). \end{aligned} \quad (2)$$

The second order Gaussian derivatives are used to build the 3×3 Hessian matrix

$$\mathbf{H} = \begin{pmatrix} I_{xx} & I_{xy} & I_{xz} \\ I_{yx} & I_{yy} & I_{yz} \\ I_{zx} & I_{zy} & I_{zz} \end{pmatrix}. \quad (3)$$

Arguments are left out here for brevity.

From $\mathbf{H}$ we calculate the eigenvalues $\lambda_t, \lambda_n, \lambda_m$ and the corresponding eigenvectors $\mathbf{t}$, $\mathbf{n}$ and $\mathbf{m}$ which form the orthonormal base for a local Cartesian coordinate system. The vector $\mathbf{t}$ which is aligned to the line direction (see Fig. 1) is the eigenvector with the smallest absolute eigenvalue λ_t (Koller et al., 1995; Lorenz et al., 1997).

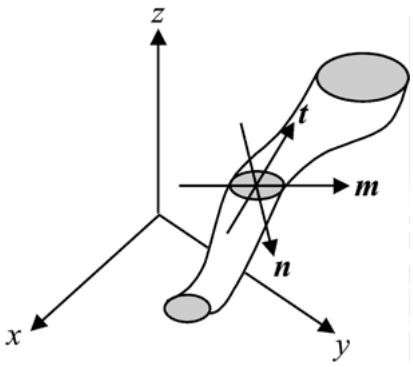

Figure 1. 3D line structure with local eigenvectors **t**, **n** and **m** of the Hessian Matrix. The eigenvector **t** with the smallest eigenvalue in magnitude is in the local direction of the line.

In the plane perpendicular to the line direction the gray value distribution can be approximated by a second order Taylor polynomial

$$I(\xi, \eta) = I + \mathbf{p} \cdot \nabla I + \frac{1}{2}\mathbf{p}^{\mathbf{T}} \cdot \mathbf{H} \cdot \mathbf{p}. \qquad (4)$$

In Eq. (4) **p** is a vector in the plane defined by **n** and **m** i.e.

$$\mathbf{p} = \xi \mathbf{n} + \eta \mathbf{m}. \qquad (5)$$

I and ∇I are the gray value and gradient vector at the current position. The position of the center line $\mathbf{P_c}$ relative to the current position $\mathbf{P_d}$ is found by setting the gradient of the local Taylor polynomial to zero (Steger, 1998)

$$\nabla I(\xi, \eta) = \mathbf{0} \qquad (6)$$

and solving η and ξ from the resulting linear equation. The actual subvoxel center line position $\mathbf{P_s}$ is calculated by

$$\mathbf{P_s} = \mathbf{P_d} + \mathbf{P_c}. \qquad (7)$$

In a discrete image $\mathbf{P_s}$ will in general not be within the boundaries of the current voxel position $\mathbf{P_d}$. If that is the case the line point estimation procedure will be carried out again at the discrete voxel position closest to $\mathbf{P_s}$. This procedure will be repeated until the subvoxel centerline position $\mathbf{P_s}$ is within the boundaries of the current voxel. The tracing proceeds by taking a step from the estimated position $\mathbf{P_s}$ in the **t**-direction and estimating a new position $\mathbf{P_s}$ as described above.

Note that occasionally the iterative procedure to find the center line position may not converge. This problem can be avoided by centering the differentiation kernel at the estimated subvoxel position after each iteration step.

The tracing procedure for the 3D curvilinear structures described here can also be used for curves in 2D images. In that case all 3D vectors and matrices appearing in this section are replaced by their 2D counterparts.

2.2. *Curvature Induced Bias in Line Center Position*

From scale space theory it is known that the position of a critical point like an extremum or saddle point in an image is dependent on the scale at which the image is observed (Lindeberg, 1992; Kuijper and Florack, 1999). As a function of scale the critical point is moving along a trajectory in the N-dimensional space of the image. Since a line point in a N-dimensional image is an extremum in the $N-1$ dimensional sub space perpendicular to the line direction (Staal et al., 1999) it is expected that the positions of the center line points shift as a function of scale. In straight symmetric lines we observed no significant shift due to the isotropic properties of the differentiation kernels (Streekstra et al., 1999). If the line is curved a bias from the true line positions is observed (Streekstra et al., 2000).

Starting point in our analysis of the scale dependent position of center line points in space is a first order Taylor expansion of the gradient. As shown in (Kuijper and Florack, 1999) the Taylor expansion of the gradient in position and scale is given by

$$\nabla I(\mathbf{p_0} + \delta\mathbf{p}, s_0 + \delta s) = \mathbf{H}(\mathbf{p_0}, s_0) \cdot \delta\mathbf{p} + \mathbf{w}(\mathbf{p_0}, s_0)\, \delta s. \qquad (8)$$

In (8), **p** is an arbitrary position in space, s is the scale parameter ($s = \frac{1}{2}\sigma^2$) and $\mathbf{p_0}$ a critical point at scale s_0. The matrix $\mathbf{H}(\mathbf{p_0}, s_0)$ is the Hessian matrix, $\mathbf{w}(\mathbf{p_0}, s_0) = \triangle(\nabla I(\mathbf{p_0}, s_0))$ and $\triangle$ denotes the Laplacian operator. Setting the left part of (8) to zero yields the first order approximation relating the shift $\delta\mathbf{p}$ in position of the critical point to a variation δs in scale. In our analysis we choose $s_0 = 0$ and p_0 at the center line of the curvilinear structure. Using (8) we can calculate the shift in line center position when the scale increases.

To investigate the bias in center line position due to line curvature and scale we model a curved line structure by a circle of a certain thickness in a 2D image.

The center of mass of the circle is in the origin. The radius of curvature is given by R_t and R is the radius of the intensity profile across the line (Fig. 2).

Because of the circular symmetry of the line structure it is most convenient to use polar coordinates for the calculation of the scale dependent line center shift. The coordinate transformation relating polar coordinates to Cartesian is given by

$$\begin{aligned} x &= \rho \cos\theta \\ y &= \rho \sin\theta \end{aligned} \tag{9}$$

In a circular symmetrical object all derivatives with respect to θ vanish and we have for the first order derivative operators

$$\begin{aligned} \frac{\partial}{\partial x} &= \cos\theta \frac{\partial}{\partial \rho} \\ \frac{\partial}{\partial y} &= \sin\theta \frac{\partial}{\partial \rho}, \end{aligned} \tag{10}$$

and for the Laplacian Δ

$$\Delta = \frac{\partial^2}{\partial \rho^2} + \frac{1}{\rho}\frac{\partial}{\partial \rho}. \tag{11}$$

Since we are interested in the shift within the 1D subspace perpendicular to the line direction, at constant θ, $\delta\mathbf{p}$ is given by

$$\delta\mathbf{p} = \begin{pmatrix} \delta\rho \cos\theta \\ \delta\rho \sin\theta \end{pmatrix}. \tag{12}$$

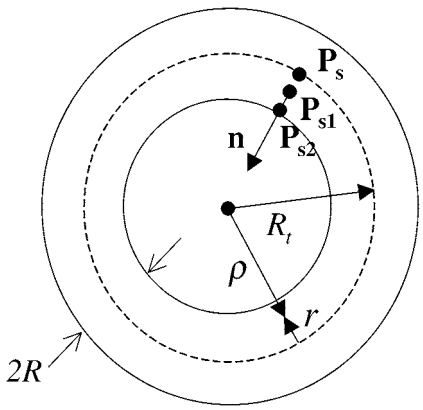

Figure 2. Circle with radius of curvature R_t and radius R of the intensity profile across the line. Centerline positions $\mathbf{P_{s1}}$ and $\mathbf{P_{s2}}$ are obtained at scales σ_1 and σ_2 respectively. $\mathbf{P_s}$ is the unbiased centerline position at $\sigma = 0$.

Using (10) and (11) for the calculation of the derivatives appearing in (8) and using (12) for $\delta\mathbf{p}$ we arrive at the equation relating $\delta\rho$ and δs

$$\left(\frac{\partial^2 I}{\partial \rho^2}\right)\delta\rho + \left(\frac{\partial^3 I}{\partial \rho^3} + \frac{1}{\rho}\frac{\partial^2 I}{\partial \rho^2}\right)\delta s = 0. \tag{13}$$

Arguments are left out here for brevity.

To materialize the relationship between $\delta\mathbf{p}$ and δs from (13) we need expressions for the partial derivatives with respect to ρ at the center line of the original object ($s = 0$). These expressions are governed by the shape $f(r)$ of the line profile at zero scale. We assume that the intensity profile is bounded by the general condition

$$I(r) = \begin{cases} I_0 f(r), & (r \le R) \\ 0, & (r > R). \end{cases} \tag{14}$$

In Eq. (14) I_0 is the gray value at the center line, $r = \rho - R_t$ represents the radial position relative to the center line and R is the radius of the line structure. We demand that the first derivative of $f(r)$ vanishes at the centerline. Since we don't want to be limited to only one single line profile type we perform the analysis for a general profile type $f(r)$ given by:

$$f(r) = \frac{\left(1 - e^{-\alpha(\frac{r}{R}+1)}\right)\left(1 - e^{\alpha(\frac{r}{R}-1)}\right)}{(1 - e^{-\alpha})^2} \tag{15}$$

Figure 3 shows that by changing α the shape of the profile can be adjusted. The line profiles corresponding

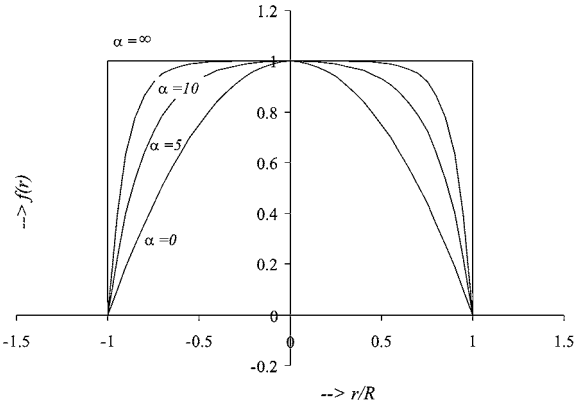

Figure 3. Shape of the line profile for different values of α. The shape of the profile changes from parabolic for $\alpha \to 0$ to pillbox shaped for $\alpha \to \infty$.

to the limiting cases $\alpha \to 0$ and $\alpha \to \infty$ are a parabolic and a bar profile respectively.

For the general profile described by (15) the third order partial derivative in (13) vanishes for points at the center line ($\rho = R_t$). Only $\frac{\partial^2 I}{\partial \rho^2}$ turns out to be nonzero yielding a simple relationship between $\delta\rho$ and s

$$\delta\rho = -\frac{s}{R_t}. \tag{16}$$

Equation (16) reveals that the shift $\triangle P_s = -\delta\rho$ is towards the center of mass of the circular line structure and independent of the radius R of the line profile.

In practice the parameter of interest will be the shift normalized with respect to R. From (16) we can write the normalized shift $\triangle P_s/R$ in terms of σ/R_t and σ/R:

$$\frac{\triangle P_s}{R} = \frac{1}{2}\frac{\sigma^2}{RR_t}. \tag{17}$$

In 3D images it is appropriate to locally model an arbitrary 3D curvilinear structure by a helix. In the derivation of the shift-scale relationship in 3D we choose the helix to be winding along the z-axis of a Cartesian coordinate system. The center line positions can be parameterized by the polar angle θ i.e.

$$\mathbf{p}(\theta) = (R_t \cos\theta, R_t \sin\theta, A\theta)\cdot \tag{18}$$

In (18) R_t is the radius of the cylinder which comprises the center line of the helix and A is the pitch of the helix. For this helix both curvature and torsion are constant:

$$\begin{aligned} \kappa &= \frac{R_t}{R_t^2 + A^2}, \\ \tau &= \frac{A}{R_t^2 + A^2}. \end{aligned} \tag{19}$$

As in the 2D case the center line is considered to be surrounded by a general intensity profile described in Eq. (15).

In the Appendix the relationship between the line center shift and scale is derived for a helical line structure. Apart from the scale parameter s the center line shift turns out to be dependent on both local curvature κ and torsion τ:

$$\Delta P_s = \kappa\left(1 - \left(\frac{\tau}{\kappa}\right)^2 - 2\left(\frac{\tau}{\kappa}\right)^4\right)s. \tag{20}$$

Similar to the derivation in the appendix one can prove that (20) also holds for a Gaussian intensity profile across the line:

$$I(r) = I_0 e^{-\frac{1}{2}\frac{\sigma^2}{R^2}} \tag{21}$$

It is easily verified that if $\tau = 0$ (20) reduces to its 2D counterpart (16). This means that if the 3D curvilinear structure is a torus ($\tau = A = 0, \kappa = \frac{1}{R_t}$) the relationship between scale and center line shift is the same as for a 2D circle.

From (20) can be concluded that for a helix with $\tau > 0$ the slope of the linear relationship between $\Delta R/R$ and $\frac{1}{2}\frac{\kappa}{R}\sigma^2$ is not 1 as for the torus and the circle. The slope $y(\tau/\kappa)$ is a function of τ/κ i.e.:

$$\frac{\Delta P_s}{R} = y(\tau/\kappa)\frac{1}{2}\frac{\kappa}{R}\sigma^2. \tag{22}$$

with

$$y(\epsilon) = (1 - \epsilon^2 - 2\epsilon^4). \tag{23}$$

Figure 4 shows that the slope $y(\tau/\kappa)$ is close to 1 for small τ/κ fractions where the helix closely resembles the shape of a torus. For lager τ/κ fractions $y(\tau/\kappa)$ decreases. The shift is directed towards the center of the helical axis as long as $\tau/\kappa < \frac{1}{2}\sqrt{2}$. For $\tau/\kappa > \frac{1}{2}\sqrt{2}$ the slope $y(\tau/\kappa) < 0$ implying a shift which is directed from the central axis of the helix. At $\tau/\kappa = \frac{1}{2}\sqrt{2}$ the centerline shift vanishes.

2.3. *Bias Removal and Curvature Measurement*

In curved line structures the bias in the centerline position ΔP_s can become in the order of several pixels or

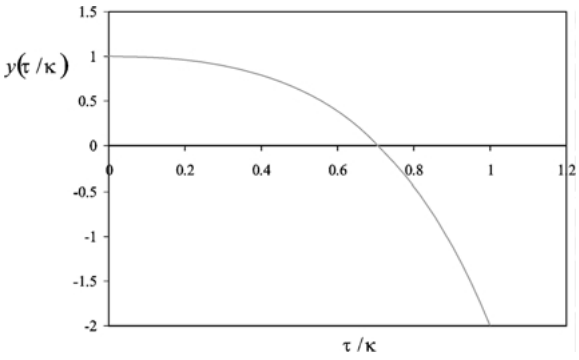

Figure 4. The slope $y(\tau/\kappa)$ of the linear relationship between $\Delta R/R$ and $\frac{1}{2}\frac{\kappa}{R}\sigma^2$ for a helical structure.

voxels. For these cases the availability of a method to reduce this bias is desirable.

The correction procedure which we propose starts by calculating $\mathbf{P_s}$ at two scales σ_1 and σ_2 with corresponding centerline positions $\mathbf{P_{s1}}$ and $\mathbf{P_{s2}}(\sigma_2 > \sigma_1)$. From $\mathbf{P_{s1}}$ and $\mathbf{P_{s2}}$ it is possible to calculate the normal vector $\mathbf{n}$ which points towards the center of mass of the circle (Fig. 2).

$$\mathbf{n} = \frac{\mathbf{P_{s2}} - \mathbf{P_{s1}}}{|\mathbf{P_{s2}} - \mathbf{P_{s1}}|}. \tag{24}$$

For a circle in 2D and a torus in 3D equation (16) implies that $\mathbf{n}$ is pointing towards the center of mass of the object. Applying Eq. (16) to these objects it is straightforward to show that the distance between two position vectors $\mathbf{P_{s1}}$ and $\mathbf{P_{s2}}$ is given by

$$|\mathbf{P_{s2}} - \mathbf{P_{s1}}| = \frac{\sigma_2^2 - \sigma_1^2}{2R_t}. \tag{25}$$

The value of R_t is found by solving (25) for R_t

$$R_t = \frac{\left(\sigma_2^2 - \sigma_1^2\right)}{2|\mathbf{P_{s2}} - \mathbf{P_{s1}}|}. \tag{26}$$

The corrected $\mathbf{P_s}$ is found by subtracting the shift along $\mathbf{n}$ at scale σ_i from the estimated $\mathbf{P_{si}}$, i.e.

$$\mathbf{P_s} = \mathbf{P_{si}} - \frac{\sigma_i^2}{2R_t}\mathbf{n} \quad (i = 1, 2). \tag{27}$$

The generalization of the bias removal method to a helical line structure is straightforward since in the 3D case the line center shift is also proportional to σ^2 (cf. Eq. (22)). The only difference is that the $\frac{1}{2R_t}$ fraction in (17) is replaced by $\frac{\kappa}{2}(1-(\frac{\tau}{\kappa})^2-2(\frac{\tau}{\kappa})^4)$ and the direction of the shift is in the osculating plane comprising the tangent and the normal vectors of the helix. In a helical line structure it is not possible to obtain τ or κ with the procedure described in this section.

2.4. Tracing and Curvature Measurement in Images

To validate (17) we performed localization experiments in 2D synthetic images of circles by measuring ΔP_s as a function of scale. In each localization experiment all line center positions within a circular object were obtained by the tracing method described in Section 2.1. In all cases the variation in the measured ΔP_s is negligible compared to the average bias introduced by the curvature. Values of R_t/R of 3, 5 and 10 were chosen to represent a highly, a moderately and a slightly curved line structure respectively. In all experiments the line profile was chosen to be parabolic and R was set to 5 pixels.

Figure 5 shows the result of the localization experiments. Independent of the value of R_t/R the experimentally obtained center line shift corresponds to the theoretical value approximately up to $\frac{1}{2}\frac{\sigma^2}{RR_t} = 0.2$.

To verify the conclusion that the relationship between scale and center line shift for a torus is the same as for a 2D circle experiments on center line shifts in a toroidal object were performed. Values of R_t/R of 3, 5 and 10 were chosen to represent a highly, a moderately and a slightly curved line structure respectively. For R we chose the values 3, 5 and 10. The profile shape parameter α was varied between 0 and 10 in order to cover a large range of profile types between a parabolic profile and a pillbox profile. The results of the localization experiments show the same shift-scale relationship for all α both in shape and magnitude. Figure 6 shows the results on profiles with $\alpha = 0$ (parabolic profile) and $\alpha = 5$.

As in the experiments with the 2D circle (Fig. 5) the first order approximation holds for values of $\frac{1}{2}\frac{\sigma^2}{RR_t}$ up to 0.2. At values of $\frac{1}{2}\frac{\sigma^2}{RR_t} > 0.2$ higher order terms in scale parameter s will play a role in the actual shift-scale relationship.

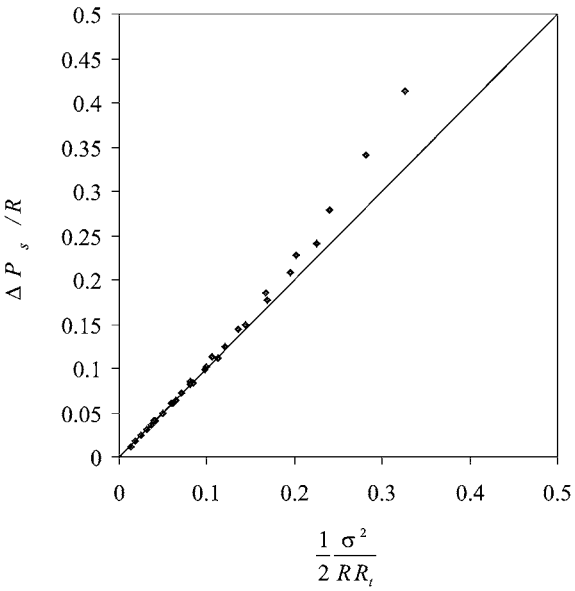

Figure 5. $\Delta P_s/R$ as function of $\frac{1}{2}\frac{\sigma^2}{RR_t}$ for a parabolic profile. The solid straight line shows the theoretical first order relationship between scale and center line shift.

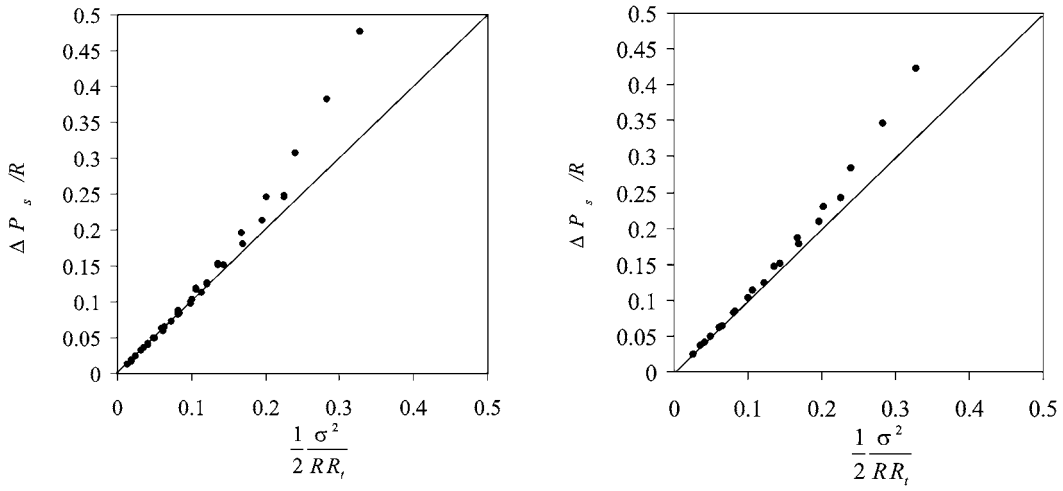

Figure 6. $\Delta P_s/R$ as function of $\frac{1}{2}\frac{\sigma^2}{RR_t}$ in a toroidal object for a parabolic profile (left panel) and for a profile with shape parameter $\alpha = 5$ (right panel). The solid straight line shows the theoretical first order relationship between scale and center line shift.

To investigate the range of validity of (22) for 3D curvilinear structures we performed localization experiments in synthetically created 3D images of helical objects. In all investigated helices κ was kept constant at a value of 0.01. For τ/κ values of 0.25, 0.56, $\frac{1}{2}\sqrt{2}$ and 0.88 were chosen corresponding to slopes $y(\tau/\kappa)$ of 0.93, 0.5, 0 and -1 respectively. The intensity profile across the line was chosen to be Gaussian with $R = 20$.

The results of the localization experiments (Fig. 7) show the validity of Eq. (22) within the range of scales investigated. For $\tau/\kappa = 0.25$ the simulation results are in agreement with the theory. For larger τ/κ the measured shift-scale relationship deviates from the theory. However, the simulation show that the general mechanisms predicted by our first order approximation hold: at $\tau/\kappa = \frac{1}{2}\sqrt{2}$ the shift almost vanishes and for $\tau/\kappa > \frac{1}{2}\sqrt{2}$ the inversion in the shift direction is clearly observed.

The bias correction method was evaluated using synthetical images of toroidal objects. Figure 8 shows an example of the performance of the method ($\sigma/R = 1$). After correction the relative bias $\Delta P_s/R$ is negligible for relative curvature $R_t/R > 3$ which is in correspondence with the theory (cf. Fig. 6). We found similar results for different choices of the scale parameters provided that they are within the range usually applied in scale space methods.

The applicability of the tracing method and curvature measurement in real images is illustrated in two different examples of 3D biological curvilinear structures (Fig. 9). The images were obtained using a confocal microscope. The experiments reveal that the center line estimation method converges to the optimal center line position as long as the scale of the differentiation kernels was chosen larger than the radius R of the intensity profile across the line. Taking this constraint imposed on the scale into account the method is capable of measuring center line positions even in the noisy image of the neuron cell (Fig. 9, right image). In the image of the Spathiphyllum pollen grain (Fig. 9, left image) the method allows for tracing highly curved line segments.

Figure 10 (left panel) shows an enlarged part of the Spathiphyllum pollen grain where the center line shift due to curvature is clearly visible ($\sigma/R \approx 2$). The center line shift can actually be compensated for by applying the method as described in the previous section (Fig. 10, central panel). The radius of curvature R_t which is estimated during the compensation method is visualized by drawing the osculating circle at the center line position with the highest curvature (Fig. 10, right panel). Since $\sigma^2/2R_t \approx 0.33$ the relative center line shift $\Delta P_s/R$ is approximately 0.3 which is slightly outside the linear regime (cf. Fig. 5). Still the method performs reasonably well under these sub optimal circumstances.

3. Diameter Estimation

3.1. Single Scale Diameter Measurement

For diameter estimation it is necessary to take the shape of the 2D gray value profile perpendicular to the line

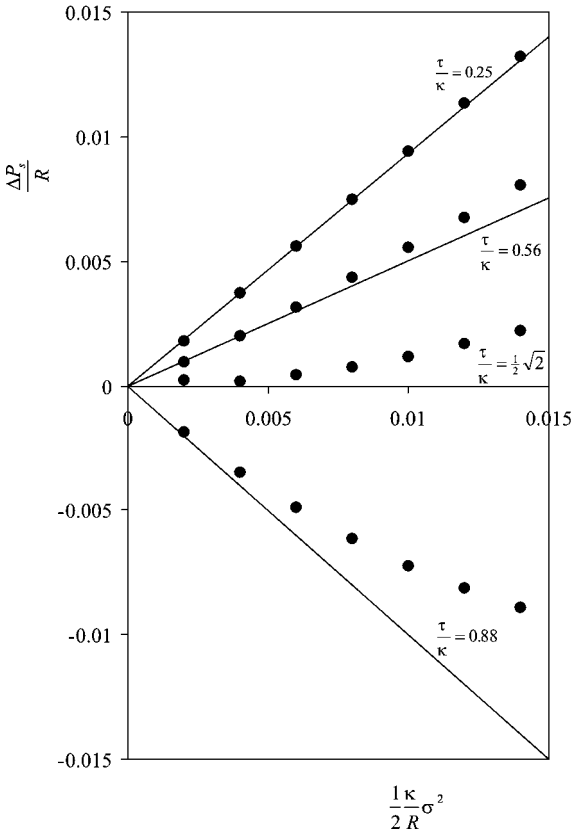

Figure 7. Relationship between $\frac{1}{2}\frac{\kappa}{R}\sigma^2$ and $\frac{\Delta P_s}{R}$ for helices of different $\frac{\tau}{\kappa}$ ratios. In all experiments κ was kept constant ($\kappa = 0.01$). The solid lines represent the theoretical first order Taylor approximations of the shift-scale relationships for the corresponding $\frac{\tau}{\kappa}$ ratios. Results on simulated images (markers) illustrate the range of validity of the approximation. $\Delta P_s > 0$ as long as the shift is directed inwards towards the axis of the helical structure.

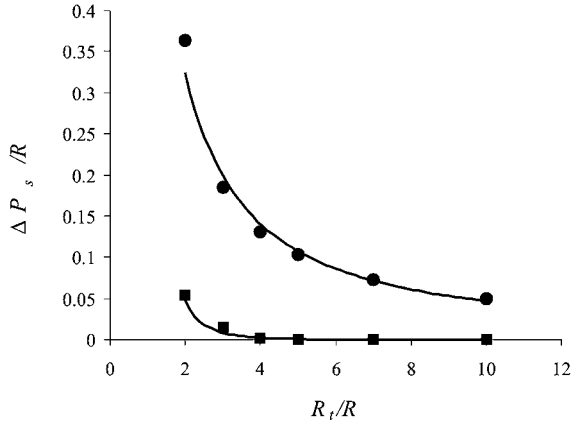

Figure 8. Correction for bias introduced by curvature. Both the bias as a result of the tracing procedure (dots, $\sigma_1/R = 1$) and the bias after correction (squares) are shown. For σ_2 a value of $1.5\sigma_1$ was chosen.

into account (Lorenz et al., 1997). The profile is assumed to obey the general condition as mentioned in (14).

We use the scale dependencies of $I(r)$ convolved with a Gaussian and the second Gaussian derivatives of $I(r)$ at $r = 0$ to estimate the line diameter. For this purpose expressions are derived for the Gaussian blurred intensity $I(R,\sigma)$ and the Laplacian $\Delta^{\perp} I(R,\sigma)$ restricted to the span of **n** and **m**:

$$I(R,\sigma) = I_0 \int_0^{2\pi}\int_0^{R} f(r) g(r,\sigma) r \, dr \, d\theta \tag{28}$$

$$\Delta^{\perp} I(R,\sigma) = I_0 \int_0^{2\pi}\int_0^{R} f(r) g_{rr}(r,\sigma) r \, dr \, d\theta. \tag{29}$$

In (28) and (29) $g(r,\sigma)$ and $g_{rr}(r,\sigma)$ are the 2D Gaussian and its second derivative in r-direction. The expressions for $I(R,\sigma)$ and the Laplacian $\Delta^{\perp} I(R,\sigma)$ are used to construct a non-linear filter which is rotation invariant with respect to the line direction and independent of I_0:

$$h(R,\sigma) = -\frac{I(R,\sigma)}{\sigma^2 \frac{1}{2}\Delta^{\perp} I(R,\sigma)}. \tag{30}$$

The denominator in (30) represents the 2D Laplacian based on normalized second derivatives (Lindeberg, 1994).

The theoretical filter output $h(R,\sigma)$ is dependent on the choice of $f(r)$. For a parabolic and a pillbox profile the integrals appearing in (28) and (29) can be evaluated analytically. For a pillbox profile we find

$$h(q) = \frac{(1 - e^{-q})}{(qe^{-q})} \tag{31}$$

and for a parabolic profile

$$h(q) = \frac{(1 - e^{-q}) - q}{(qe^{-q}) - (1 - e^{-q})} \tag{32}$$

with

$$q = \frac{1}{2}\left(\frac{R}{\sigma}\right)^2. \tag{33}$$

Equations (31)–(33) show that for the pillbox and the parabolic profile $h(R,\sigma)$ is only dependent on the dimensionless parameter q. Figure 11 shows that $h(q)$

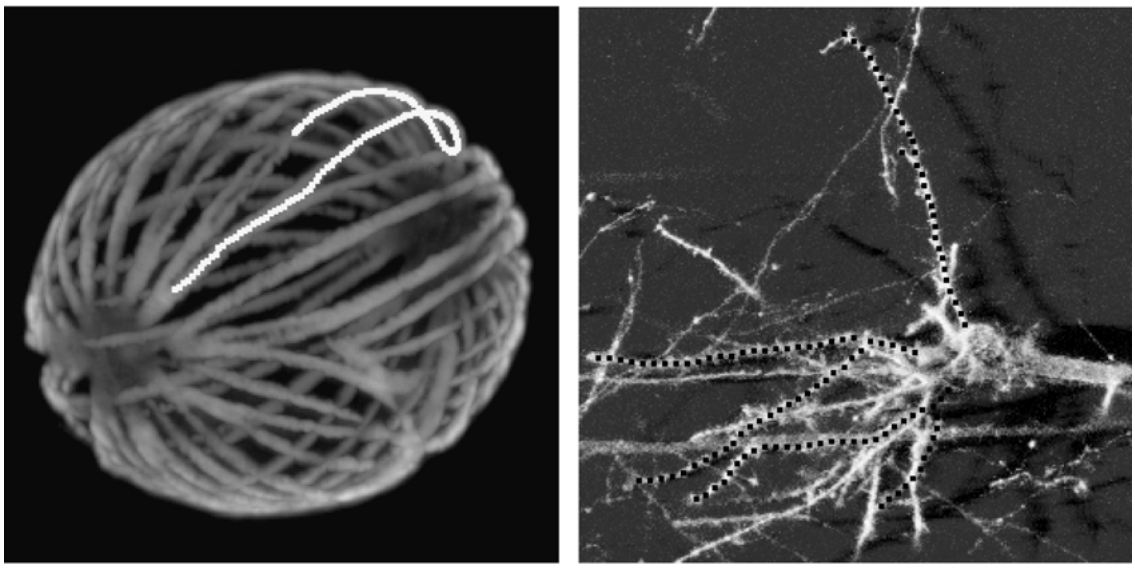

Figure 9. Tracing results in 3D images of biological specimen (left: a Spathiphyllum pollen grain, right: a pyramidal neuron cell). The images were obtained using a confocal microscope. The black dots in the right panel represent the estimated center line positions.

Figure 10. Center line shift and curvature measurement in an enlarged part of the Spathiphyllum pollen grain. The center line shift (left panel) is compensated for (central panel) using the theoretical relationship between scale and center line position. The same relationship is utilized to the measure local radius of curvature R_t of the line (right panel). The osculating circle with radius R_t is plotted in the image.

is monotonous increasing functions of q. This property makes it easy to estimate q from a measured filter output h_{meas}. If h_{meas} and the shape of the profile are known q can be estimated by solving one of the equations

$$h(q) - h_{\text{meas}} = 0. \tag{34}$$

By a simple bi-sectioning method the root q_0 of (34) is found. The corresponding R is found using by solving (33) i.e.

$$R = \sigma\sqrt{2q_0}. \tag{35}$$

3.2. Experiments on Diameter Measurement

To evaluate the performance of the line diameter estimation method synthetic images containing straight line segments with circular cross section were used. The diameter of the line segment was varied between 2 and 15. Both a pillbox shaped and a parabolic intensity profiles were evaluated. The diameter estimate turned out to be independent of the setting of σ in the range where $0.2 < R/\sigma < 2$. In the synthetic images the bias in the estimated diameter is always below 5% (see Fig. 12).

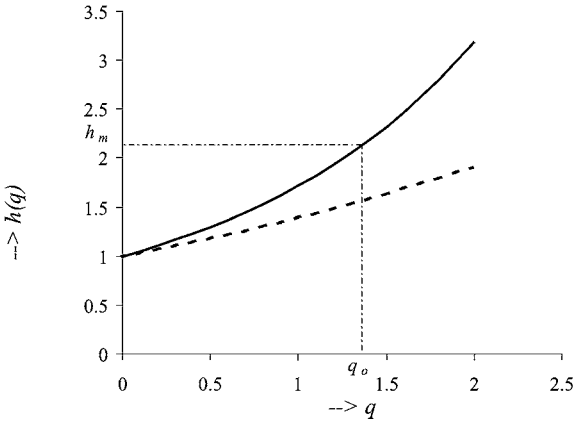

Figure 11. Theoretical line diameter filter output $h(q)$ for a pillbox profile (solid line) and a parabolic profile (dashed line). Parameter q is dimensionless and only dependent on R and $\sigma (q = \frac{1}{2}(R/\sigma)^2)$.

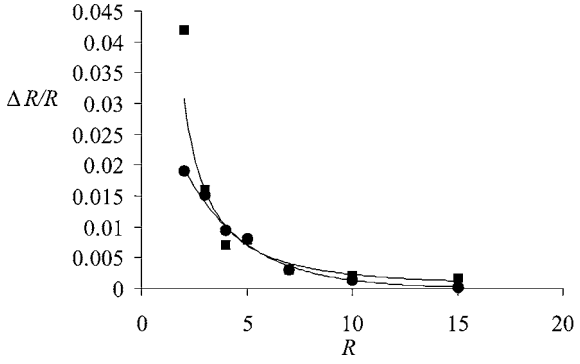

Figure 12. Relative bias in estimation of radius R of the line structure as a function of R.

The diameter measurement procedure was also tested on a biological 3D image from a confocal microscope containing a Spathiphyllum pollen grain (Fig. 9, left panel). The diameter was measured at scales varying between 2.0 and 5.0. Within this range of scales the diameter measurement deviates only 6% for the parabolic profile as a model used (Fig. 13). In case the pillbox profile is used the diameter measurement fails.

4. Discussion

We demonstrated that the information contained in the scale dependency of features based on Gaussian image derivatives can be successfully employed in quantitative measurements. Within this approach it turned out to be beneficial to combine feature measurements at multiple scales and link them to their theoretical scale relationships. In the example of curvilinear structures

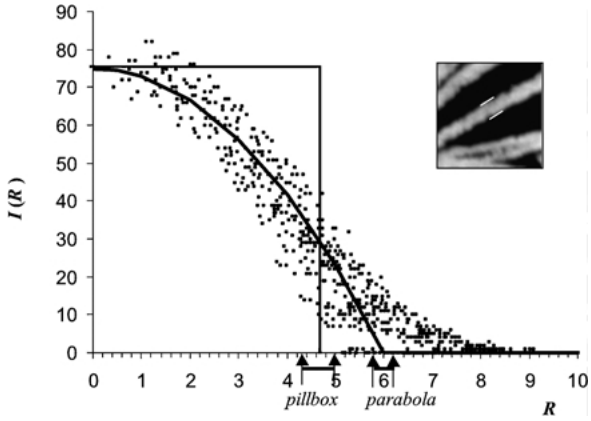

Figure 13. Results of diameter measurement in the Spathiphyllum pollen grain as compared to the intensity profile across the line. The scale was varied between 2.0 and 5.0. The vertical arrows along the x-axis indicate the outer limits of the range of the diameter measurements using a pillbox profile (left) and a parabolic profile (right).

we illustrated the applicability of our approach in measurement of features like center line position, curvature and diameter.

In our considerations so far we did not take the fractal nature of natural images into account. In a fractal object a correct scale at infinite resolution is not defined since details and repetitive structures might become arbitrary small. In practise, however, all imaging systems have a finite resolution. Consequently, the image never contains an exact reproduction of the object at hand but represents a blurred representation of the object. The results presented in this paper are limited to the representation of the object as it appears in the acquired image.

In the derivation of the bias removal method a procedure to measure local curvature of the center line naturally appears. After measuring the sub pixel center line position $\mathbf{P_s}$ at two different scales equation (26) can be used to compute R_t. The osculating circle plotted in Fig. 10. (right panel) indicates the correctness of the curvature measurement. It is of great importance to have a procedure for measurement of curvature at center line positions since it is not possible to use the usual isophote curvature (van Vliet, 1993). Although a center line is an isophote it is not possible to use the gradient based isophote curvature because the gradient is zero and has no direction at the center line. Additionally, isophote curvature measurement is carried out at a single scale which yields derivatives which are a weighted average of the actual derivatives in the neighborhood of the point of observation. This is a prominent example

of how measurement at a single scale fails and the approach as presented in this paper solves the conflict between noise suppression and measurement accuracy.

In 2D images the bias removal and R_t measurement procedures are applicable to a large class of symmetrical line profiles. Equation (13) implicates that the only restriction to the line profile of the original object is that $\frac{\partial^3 I}{\partial \rho^3} = 0$ at the center line position. In the sub-class of profiles described by Eq. (15) $\frac{\partial^3 I}{\partial \rho^3}$ will vanish at the center line. This sub-class is expected to be sufficiently general to cover the majority of profiles encountered in practice.

In a torus where $\tau/\kappa = 0$ the simple shift-scale relationship expressed in (16) is valid for the family of line profiles given by (15). The validity of (16) can even be extended by examining Eq. (52) of the appendix more closely. From this equation we conclude that Eq. (16) holds in all tori with a line profiles for which the third order derivatives and the mixed second derivatives vanish at the center line.

In the experiments shown in this paper the bias correction method turns out to be applicable in practice. Due to the extend of the Gaussian derivative kernels the method is obviously limited to curvilinear structures that are more or less isolated from surroundings structures. In case neighboring structures are within the reach of the derivative kernels the correction method is expected to perform less accurately.

In the diameter measurement procedure a priori knowledge of the shape of the intensity profile across the line is required for correct diameter measurement. An incorrect line profile model might induce a bias in the measured diameter. Measurements in Confocal Microscope Images reveal that in the extreme case in which a pillbox profile would be used in the diameter measurement of a profile which is actually parabolic, the bias is about 25 percent (cf. Fig. 13). This can be considered the maximum possible bias in this method when no a priory information on the profile shape is available.

We presented methods for feature measurement in images containing curvilinear structures. The scale dependency of the derivatives at the center line position proved to be crucial for accurate center line localization and for measurement of curvature and diameter.

Appendix

Here we derive the relationship between line center shift and scale for a helical line structure. We choose the helix to be winding along the z-axis of a Cartesian coordinate system. In that case the center line positions can be parameterized by the polar angle θ i.e.

$$\mathbf{p}(\theta) = (R_t \cos\theta, R_t \sin\theta, A\theta). \tag{36}$$

In (36) R_t is the radius of the cylinder which comprises the center line of the helix and A is the pitch of the helix. To describe a helical line structure in which the center line is surrounded by an circular symmetrical line profile we need an expression for the distance r to the center line at an arbitrary position in space. Because of the parameterization of the helix with the polar angle θ it is most convenient to change to cylindrical coordinates:

$$\begin{aligned} x &= \rho \cos\theta \\ y &= \rho \sin\theta \\ z &= z. \end{aligned} \tag{37}$$

Within this coordinate system the distance to the center line is given by:

$$r(\rho, \theta, z) = \sqrt{(\rho - R_t)^2 + (z - A\theta)^2}. \tag{38}$$

The complete 3D description of the helical line structure is given by:

$$I(r(\rho,\theta,z)) = \begin{cases} I_0 f(r(\rho,\theta,z)), & (r(\rho,\theta,z) \le R) \\ 0, & (r(\rho,\theta,z) > R). \end{cases} \tag{39}$$

In Eq. (39) I_0 is the gray value at the center line, R the radius of the line structure and $f(r(\rho,\theta,z))$ describes the shape of the intensity profile across the line.

The starting point for derivation of the relationship between line center shift and scale is Eq. (8)

$$\nabla I(\mathbf{p_0} + \delta\mathbf{p}, s_0 + \delta s) = \mathbf{H}(\mathbf{p_0}, s_0) \cdot \delta\mathbf{p} + \mathbf{w}(\mathbf{p_0}, s_0)\, \delta s. \tag{40}$$

Since we changed to cylindrical coordinates we have to express the derivatives appearing in (40) in ρ, θ and z. For this purpose we need the relationship between derivatives in a Cartesian coordinate system and a cylindrical coordinate system:

$$\frac{\partial}{\partial x} = \cos\theta \frac{\partial}{\partial \rho} - \frac{\sin\theta}{\rho} \frac{\partial}{\partial \theta} \tag{41}$$

$$\frac{\partial}{\partial y} = \sin\theta\frac{\partial}{\partial\rho} + \frac{\cos\theta}{\rho}\frac{\partial}{\partial\theta} \tag{42}$$

Based on this relationship, the Laplacian operator Δ which is used for the calculation of $\mathbf{w}(\mathbf{p_0}, s_0)$ is given by:

$$\Delta = \frac{\partial^2}{\partial\rho^2} + \frac{1}{\rho}\frac{\partial}{\partial\rho} + \frac{1}{\rho^2}\frac{\partial^2}{\partial\theta^2} + \frac{\partial^2}{\partial z^2}. \tag{43}$$

With (41)–(43) the derivation of the expressions for the derivatives appearing in (40) in cylindrical coordinates is tedious but straightforward.

Without loss of generality we restrict ourselves to the shift at the position on the centerline of the helix where $\rho = R_t$, $\theta = 0$ and $z = 0$. Leaving out the arguments of the intensity function $I(\rho, \theta, z)$ for brevity we find for the Hessian matrix $\mathbf{H}$ and for vector $\mathbf{w}$:

$$\mathbf{H} = \begin{pmatrix} \frac{\partial^2 I}{\partial\rho^2} & \frac{1}{\rho}\frac{\partial^2 I}{\partial\rho\partial\theta} - \frac{1}{\rho^2}\frac{\partial I}{\partial\theta} & \frac{\partial^2 I}{\partial\rho\partial z} \\ \frac{1}{\rho}\frac{\partial^2 I}{\partial\rho\partial\theta} - \frac{1}{\rho^2}\frac{\partial I}{\partial\theta} & \frac{1}{\rho}\frac{\partial I}{\partial\rho} + \frac{1}{\rho^2}\frac{\partial^2 I}{\partial\theta^2} & \frac{1}{\rho}\frac{\partial^2 I}{\partial\theta\partial z} \\ \frac{\partial^2 I}{\partial\rho\partial z} & \frac{1}{\rho}\frac{\partial^2 I}{\partial\theta\partial z} & \frac{\partial^2 I}{\partial z^2} \end{pmatrix} \tag{44}$$

$$\mathbf{w} = \begin{pmatrix} \frac{\partial^3 I}{\partial\rho^3} + \frac{1}{\rho}\frac{\partial^2 I}{\partial\rho^2} - \frac{1}{\rho^2}\frac{\partial I}{\partial\rho} + \frac{1}{\rho^2}\frac{\partial^3 I}{\partial\rho\partial\theta^2} - \frac{2}{\rho^3}\frac{\partial^2 I}{\partial\theta^2} + \frac{\partial^3 I}{\partial z^2\partial\rho} \\ \frac{1}{\rho}\frac{\partial^3 I}{\partial\rho^2\partial\theta} + \frac{1}{\rho^3}\frac{\partial^3 I}{\partial\theta^3} \\ \frac{\partial^3 I}{\partial\rho^2\partial z} + \frac{1}{\rho}\frac{\partial^2 I}{\partial\rho\partial z} + \frac{1}{\rho^2}\frac{\partial^3 I}{\partial\theta^2\partial z} + \frac{\partial^3 I}{\partial z^3} \end{pmatrix}. \tag{45}$$

To be able to materialize relationship between $\delta\mathbf{p}$ and δs from (40), (44) and (45) we need expressions for the partial derivatives with respect to ρ, θ and z at the center line of the original helical line structure with $s_0 = 0$. These expressions are governed by the shape $f(r(\rho, \theta, z))$ of the line profile at zero scale. We perform the analysis for a general profile type $f(r(\rho, \theta, z)))$ which is given by:

$$f(r(\rho,\theta,z)) = \frac{\left(1 - e^{-\alpha((\frac{r(\rho,\theta,z)}{R}) + 1)}\right)\left(1 - e^{\alpha((\frac{r(\rho,\theta,z)}{R}) - 1)}\right)}{(1 - e^{-\alpha})^2} \tag{46}$$

Figure 3 shows that by changing α the shape of the profile can be adjusted. By combining Eqs. (38)–(40), (44)–(46) we arrive at two independent equations relating the components of $\delta\mathbf{p}$ to the scale parameter s:

$$\delta x = -\frac{1}{R_t}\left(1 - \frac{2A^2}{R_t^2}\right)s \tag{47}$$

$$\delta z = \frac{A}{R_t}\delta y. \tag{48}$$

The latter equation shows that in this approximation only δx is dependent on s and that δz and δy are not independent. Since we are interested in the shift within the 2D sub space perpendicular to the line direction we choose $\delta\mathbf{p}$ to be directed along the x-direction (i.e. $\delta z = \delta y = 0$). We then finally find for $\Delta P_s = |\delta\mathbf{p}|$

$$\Delta P_s = \frac{1}{R_t}\left(1 - \frac{2A^2}{R_t^2}\right)s. \tag{49}$$

To adapt to the notions of curvature κ and torsion τ well established in differential geometry we can replace R_t and A for κ and τ in (49)

$$\Delta P_s = \kappa\left(1 - \left(\frac{\tau}{\kappa}\right)^2 - 2\left(\frac{\tau}{\kappa}\right)^4\right)s \ . \tag{50}$$

with

$$\kappa = \frac{R_t}{R_t^2 + A^2}$$
$$\tau = \frac{A}{R_t^2 + A^2}. \tag{51}$$

For the case that the object is a torus ($\tau = 0$) Eq. (50) reduces correctly to its 2D counterpart (16). In that case all derivatives with respect to θ vanish and we find based on (44) and (45) two independent equations relating $\delta\rho$, δz and δs

$$\begin{aligned} &\left(\frac{\partial^2 I}{\partial\rho^2}\right)\delta\rho + \left(\frac{\partial^2 I}{\partial\rho\partial z}\right)\delta z \\ &\quad + \left(\frac{\partial^3 I}{\partial\rho^3} + \frac{1}{\rho}\frac{\partial^2 I}{\partial\rho^2} - \frac{1}{\rho^2}\frac{\partial I}{\partial\rho} + \frac{\partial^3 I}{\partial z^2\partial\rho}\right)\delta s = 0 \\ &\left(\frac{\partial^2 I}{\partial\rho\partial z}\right)\delta\rho + \left(\frac{\partial^2 I}{\partial z^2}\right)\delta z \\ &\quad + \left(\frac{\partial^3 I}{\partial\rho^2\partial z} + \frac{1}{\rho}\frac{\partial^2 I}{\partial\rho\partial z} + \frac{\partial^3 I}{\partial z^3}\right)\delta s = 0. \end{aligned} \tag{52}$$

References

Bevaqua, G. and Floris, R. 1987. A surface specific-line and slope recognition algorithm. *Computer Vision, Graphics, and Image Processing*, 40:219–227.

Brakenhoff, G.J., Blom, P., and Barends, P. 1979. Confocal scanning light microscopy with high aperture immersion lenses. *J. Microscopy*, 117:219–232.

Capowsky, J.J. 1989. *Computer Techniques in Neuroanatomy*. Plenum Press: New York.

Cesar, R.M. and Da Costa, L.D. 1997. Application and assessment of multiscale bending energy for morphometric characterization of neural cells. *Rev. Sci Instr.*, 68(5):2177–2186.

Collerec, R. and Coatrieux, J.L. 1988. Vectorial Tracking and directed contour finder for vascular network in digital subtraction angiography. *Pattern Recognition Letters*, 8:353–358.

Deriche, R. and Giraudon, G. 1993. A Computational approach for corner and vertex detection. *Intern. J. Comput. Vis.*, 10(2):101–124.

Eberly, D. 1996. *Ridges in Image and Data Analysis. Computational Imaging and Vision*, Vol. 7, Kluwer Academic Publishers: Dordrecht, The Netherlands.

Florack, L.M.J., ter Haar Romeney, B.M., Koenderink, J.J., and Viergever, M.A. 1992. Scale and the structure of images. *Image and Vision Computing*, 10(6):376–388.

Frangi, A.F., Niessen, W.J., Hoogeveen, R.M., van Walsum, Th., and Viergever, M.A. 1999. Model-based quantitation of 3D magnetic resonance angiographic images. *IEEE Transactions on Medical Imaging*, 18(10):946–956.

Gonzalez, R.C. and Woods, R.E. 1992. *Digital Imaging Processing*. Addison-Wesley: Reading.

Haralick, R.M. 1983. Ridges and valleys on digital images. *Computer Vision, Graphics, and Image Processing*, 22:28–38.

Houtsmuller, A.B., Smeulders, A.W.M., van der Voort, H.T.M., Oud, J.L., and Nanninga, N. 1993. The homing cursor: A tool for three-dimensional chromosome analysis. *Cytometry*, 14:501–509.

Jonk, A. 1997. A line tracker. Internal ISIS report, Amsterdam University.

Koenderink, J.J. and van Doorn, A.J. 1994. Two-plus-one-dimensional differential geometry. *Pattern Recognition Letters*, 15(5):439–443.

Koller, Th.M., Gerig, G., Szekely, G., and Dettwiler, D. 1995. Multiscale detection of curvilinear structures in 2-D and 3-D image data. In *Proceedings of the Fifth International Conference on Computer Vision*, pp. 864–869.

Kuijper, A. and Florack, L.M.J. 1999. Calculations on critical points under Gaussian blurring. In *Proc. of the Second International Conference on Scale-Space Theories in Computer Vision*, Corfu, Greece, pp. 318–329.

Lindeberg, T. 1992. Scale-space behavior of local extrema and blobs. *Journal of Mathematical Imaging and Vision*, 1(1):65–99.

Lindeberg, T. 1994. *Scale-Space Theory in Computer Vision*. Kluwer Academic Publishers: Boston.

Lindeberg, T. 1996. Edge detection and ridge detection with automatic scale selection. In *Proc. Computer Vision and Pattern Recognition*, IEEE Computer Society Press: Los Alamitos, CA, pp. 465–470.

Lorenz, C., Carlsen, I.C., Buzug, T.M., Fassnacht, C., and Weese, J. 1997. Multi-scale line segmentation with automatic estimation of width, contrast and tangential direction in 2D and 3D medical images. In *Proceedings of the First Joint Conference on Computer Vision, Virtual Reality and Robotics in Medicine and Medical Robotics and Computer-Assited Surgery*, pp. 233–242.

Maintz, J.B.A., van den Elsen, P.A., and Viergever, M.A. 1996. Evaluation of ridge seeking operators for multimodality medical image matching. *IEEE Trans. PAMI*, 18(4):353–365.

Noordmans, H.J. 1997. Interactive analysis of 3D microscope images. Ph.D. Thesis, Amsterdam, The Netherlands.

Sato, Y., Nakajima, S., Shiraga, N., Atsumi, H., Yoshida, S., Koller, T., Gerig, G., and Kikinis, R. 1998. Three-dimensional multi-scale line filter for segmentation and visualization of curvilinear structures in medical images. *Med. Image Anal.*, 2(2):143–168.

Sporring, J., Nielsen, M., Florack, L.M.J., and Johansen, P. 1997. *Gaussian Scale-Space Theory*. Kluwer Academic Publishers: Boston.

Staal, J.J., Kalitzin, S.N., ter Haar Romeny, B.M., and Viergever, M.A. 1999. Detection of critical structures in scale space. In *Proc. of the Second International Conference on Scale-Space Theories in Computer Vision*, Corfu, Greece, pp. 105–116.

Steger, C. 1996. Extraction of curved lines from images. In *Proceedings of ICPR*, IEEE Computer Society Press: Los Alamitos, CA, pp. 251–255.

Steger, C. 1998. An unbiased detector of curvilinear structures. *IEEE Trans. PAMI*, 20(2):113–125.

Steger, C. 1998. Unbiased extraction of cuvilinear structures from 2D and 3D images. Ph.D. Thesis, Muenchen, Germany.

Streekstra, G.J., Smeulders, A.W.M., and van den Boomgaard, R. 1999. Tracing of curvilinear structures in 3D images with single scale diameter measurement. In *Proc. of the Second International Conference on Scale-Space Theories in Computer Vision*, Corfu, Greece, pp. 501–506.

Streekstra, G.J., Smeulders, A.W.M., and van den Boomgaard, R. 2000. Scale dependent differential geometry for the measurement of centerline and diameter in 3D curvilinear structures. In *Proc. of the Sixth European Conference on Computer Vision*, Dublin, Ireland, pp. 856–870.

van Vliet, L.J. 1993. Grey-scale measurements in multi-dimensional images. Ph.D. Thesis, Delft, The Netherlands.